Underactuated Virtual Gravity Control: Harnessing Passive Dynamics for Optimally Efficient Bipedal Locomotion

Aikaterini Smyrli*, *Member, IEEE*, and Evangelos Papadopoulos, *Life Fellow, IEEE*

***Abstract*—This paper explores the Underactuated Virtual Gravity (UVG) controller, a model-based control approach designed to achieve energy-efficient bipedal walking. The UVG controller minimizes actuator effort during level-ground walking by capitalizing on the inherent dynamics that facilitate stable passive gaits on downward slopes. By effectively leveraging torso dynamics to support the application of the UVG, the method turns the innate underactuation of bipedal systems into an advantage. Extensive benchmarking against state-of-the-art methods such as the Trajectory Optimization for trajectory planning combined with Non-linear Model Predictive Control for tracking shows that the UVG achieves superior energy efficiency within its effective range while constituting a closed-form controller that requires fewer computational resources than numerical methods. The results highlight the UVG and related dynamics-based approaches as a compelling option for energy-conscious, task-focused robot designs.**

I. Introduction

Bipedal locomotion control is a challenging problem that addresses the achievement of stable and efficient walking despite the inherently unstable nature of the two-legged configuration. Biped robots must coordinate multiple Degrees of Freedom (DoF) while managing their hybrid dynamics, in a state of underactuation. Control strategies seek to address these complexities while ensuring robustness and maintaining energy efficiency. Achieving this balance has led to the development of a variety of control approaches, each with distinct strengths and limitations.

Traditional model-based control methods, such as the combination of the Linear Inverted Pendulum (LIP) model with the Zero Moment Point (ZMP) criterion, have been widely used to achieve stable walking, by indicating trajectories that maintain the robot's center of mass within a confined region to ensure stability [1][2]. However, such approaches are not designed around the hybrid nature of gait dynamics and must be compensated with corrective actions after each impact.

Other approaches, such as the Model Predictive Control (MPC) can be designed to accommodate heelstrike impacts, and offer enhanced adaptability by continuously replanning to respond to disturbances in real-time [3][4]. Alternatively, methods such as the Hybrid Zero Dynamics (HZD), incorporate hybrid dynamics in their derivation, and ensure stable limit cycles for underactuated walking by imposing virtual constraints on system dynamics [5][6]. Such methods are generally not designed with energy efficiency as a priority, with methods such as Trajectory Optimization (TOPT) often incorporated alongside them to improve energetic performance [7]. While very effective, these methods are computationally intensive and their solution can be time-consuming: each step of the prediction horizon introduces a computational complexity of $\mathcal{O}(n^3)$ where n is the number of DoF [8], scaling to $\mathcal{O}(pn^3)$ over a prediction horizon p, and $\mathcal{O}(ipn^3)$ considering i iterations until convergence.

Data-driven methods such as reinforcement learning have also demonstrated promising results in enabling robust walking [9][10], allowing robots to learn complex behaviors through experience. However, these require extensive training data and generally lack interpretability.

On the other hand, passive-gait inspired controllers offer closed-form solutions to the bipedal walking control problem. Such model-based approaches are designed around the passive gaits of bipedal robots and naturally account for hybrid dynamics, making them inherently capable of handling impacts -and, in fact, reliant on them for proper function. However, they typically rely on full actuation to achieve stability [11][12][13]. Underactuated passivity-inspired approaches based on time scaling have been explored, which replicate passive trajectories in underactuated robots by modifying the timing of the motion [14][15]. These methods achieve geometric alignment with passive trajectories, but sacrifice temporal tracking, distorting the system's natural dynamics. Other approaches of underactuated passive gait have substituted gravitational pull with motor input that is aligned with the robot's design, leading to successful level-ground gait with small energy costs [17], [16]. These works showcase that gravity power is not essential to achieve passive-dynamic walking. Moreover, a common hypothesis of whether "passive-based means maximally energy effective" remains an open point [18].

In this work, we study the Underactuated Virtual Gravity (UVG) control, a closed-form, model-based control approach that leverages insights from passive gait dynamics to achieve efficient underactuated bipedal walking, firstly introduced in [19]. The developed controller replicates passive walking on level ground, and emphasizes inherent stability and minimal actuator effort by promoting joint trajectories that follow the robot's passive dynamic tendencies. Here, the effectiveness of the UVG is evaluated through a series of benchmarking experiments against state-of-the-art alternatives for energy efficiency, including TOPT and MPC-based methods. The work demonstrates that the UVG achieves superior energy efficiency within its effective range, while its closed form provides a computational advantage over numerical optimization methods: the UVG is an explicit state-feedback policy: thus

*Corresponding author.

Aikaterini Smyrli and Evangelos Papadopoulos are with HERON - Hellenic Robotics Center of Excellence, Athena Research Center, Greece. (e-mail: katerina.smyrli, egpapado@athenarc.gr). Evangelos Papadopoulos is also with the School of Mechanical Engineering, National Technical University of Athens, Greece.

each control update requires only algebraic evaluation of the feedback law, with computational cost linear in the number of states, i.e., $\mathcal{O}(n)$.

This work contributes with the finding that passivity-inspired gait may be more energy-effective than numerically optimal control solutions. The study offers valuable guidance for developing future robots that achieve improved efficiency and stability, by strategically designing systems that resonate with stable passive dynamic behaviors. The combination of this design philosophy with complementary control has the potential to unlock new possibilities for adaptable, versatile and efficient robotic locomotion.

II. Model-based UVG Controller

A. Passive walking

We consider a passive biped model, see Fig. 1a-c, which comprises two identical legs. Each leg has a femoral and a tibial link connected by a four-bar mechanism that emulates the knee constraints imposed by the cruciate ligaments [20]. Viscoelastic kneecaps at both knees prevent hyperextension during walking. The two femoral links are joined by a revolute hip joint at H. The tibial links connect rigidly to biomimetic feet designed to mimic the human foot's rollover shape [21]. The feet roll without slipping during ground contact. Each link has a mass m_j located at a distance r_j from its proximal end (closest to the hip H), a moment of inertia I_j and a total length of l_j, where $j = \{f, t\}$ for the femoral and tibial links respectively. All design parameter values are defined in [19].

The generalized coordinates of the passive biped are:

$$\mathbf{q} = [x_h, y_h, \theta_{1f}, \theta_{1k}, \theta_{2f}, \theta_{2k}]^{\mathrm{T}} \tag{1}$$

where x_h, y_h locate the hip joint H, and θ_{jf} and θ_{jk} (with $j = 1, 2$) denote the femoral and knee angles of Leg 1 and Leg 2 respectively.

The passive dynamics on a slope of angle a are expressed:

$$\mathbf{M}(\mathbf{q})\ddot{\mathbf{q}} + \mathbf{C}(\mathbf{q}, \dot{\mathbf{q}}) + \mathbf{G}(\mathbf{q}, a) - \mathbf{J}(\mathbf{q})\lambda = \mathbf{0} \tag{2a}$$

$$\mathbf{s}(\mathbf{q}) = \mathbf{0} \tag{2b}$$

$$\mathbf{J}(\mathbf{q}) = (\partial \mathbf{s}/\partial \mathbf{q})^{\mathrm{T}} \tag{2c}$$

where $\mathbf{M}$ is the 6×6 inertia matrix, $\mathbf{C}$ is 6×1 and includes Coriolis, centrifugal, and viscoelastic knee forces, $\mathbf{G}$ is 6×1 and contains gravitational forces that depend on a. Finally $\mathbf{s}(\mathbf{q})$ is $j \times 1$ and enforces the rolling constraints of the feet with j=2 in the single-stance phase (SSP), while it is $j = 4$ in the double-stance phase (DSP). $\mathbf{J}$ is the corresponding $6 \times j$ constraint Jacobian.

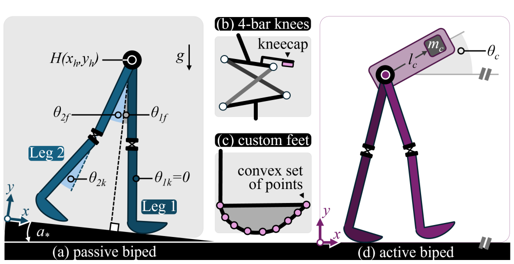

Figure 1. (a) Bio-inspired passive biped from [21] walking down a negative slope a_*, equipped with (b) 4-bar knees and (c) custom feet made up of any convex set of points to capture any geometry. (d) Active biped: a torso is added to accommodate UVG control for level-ground walking.

The Ground Reaction Force (GRF) vector λ is $j \times 1$ and can be calculated via double differentiation of the constraints $\mathbf{s}(\mathbf{q})$ in (2b) to obtain an expression for $\ddot{\mathbf{q}}$ which is then substituted in (2a) to yield:

$$\lambda = -\boldsymbol{\Delta}[\dot{\mathbf{J}}^{\mathbf{T}}\dot{\mathbf{q}} + \mathbf{J}^{\mathbf{T}}\mathbf{M}^{-1}(-\mathbf{C} - \mathbf{G} + \mathbf{u})] \tag{3a}$$

$$\boldsymbol{\Delta} \triangleq (\mathbf{J}^{\mathbf{T}}\mathbf{M}^{-1}\mathbf{J})^{-1} \tag{3b}$$

in which $\boldsymbol{\Delta}$ is the $n \times n$ operational space inertial matrix which is invertible, as $\mathbf{M}$ is positive definite and $\mathbf{J}$ is full column rank, $\mathrm{rk}(\mathbf{J}) = j$ where $\mathrm{rk}(\cdot)$ denotes the matrix rank.

On some negative slopes a_*, the passive biped of Fig. 1a can sustain a stable passive gait [20]. These a_* define the set $\mathbb{A}_*$. Eq. (2a) can then be written as:

$$\mathbf{M}\ddot{\mathbf{q}} + \mathbf{C} + \mathbf{G}_* - \mathbf{J}\lambda_* = \mathbf{0} \ , \forall a_* \in \mathbb{A}^* \tag{4}$$

in which $\mathbf{G}_*$ and λ_* are calculated for $a = a_*$. The solutions of (4) constitute steps of a cyclic passive gait on slope. In previous works [20], [21] the design of the biped walker has been optimized for passive gait efficiency, ultimately minimizing the magnitude of a_*. However, on level ground, the unactuated biped loses energy with each impact and soon collapses without the recovery that gravity provides during descent [22]. The role of gravity in sustaining a cyclic gait is thus evident from a system dynamics perspective.

B. UVG Control

In this work, we leverage the inherent passive dynamics observed when a biped descends an inclined surface, to drive level-ground walking in bipeds equipped with a torso link.

On level ground ($a = 0$), the absence of a horizontal gravitational component prevents the natural energy recovery observed on the slope. To compensate, we introduce an external torque $\mathbf{u_0}$ such that the level-ground dynamics,

$$\mathbf{M}\ddot{\mathbf{q}} + \mathbf{C} + \mathbf{G_0} - \mathbf{J}\lambda_{\mathbf{0}} = \mathbf{u_0} \tag{5}$$

mimic the passive walking behavior on the slope a_*. Here $\mathbf{G_0}$ and $\lambda_{\mathbf{0}}$ are calculated using $a = 0$.

Matching the trajectories requires that $\mathbf{q}$, $\dot{\mathbf{q}}$ and $\ddot{\mathbf{q}}$ remain the same in both cases. Subtracting the passive dynamics of (4) from the level-ground dynamics of (5) yields:

$$(\mathbf{G_0} - \mathbf{G}_*) + \mathbf{J}(\lambda_* - \lambda_{\mathbf{0}}) = \mathbf{u_0} \tag{6}$$

Using (3) to substitute λ and $\lambda_{\mathbf{0}}$ in (6) leads to:

$$\mathbf{A}(\boldsymbol{\Gamma} - \mathbf{u_0}) = \mathbf{0} \tag{7a}$$

$$\mathbf{A} \triangleq \mathbf{I} - \mathbf{J}\boldsymbol{\Delta}\mathbf{J}^{\mathbf{T}}\mathbf{M}^{-1} \tag{7b}$$

$$\boldsymbol{\Gamma} \triangleq \mathbf{G_0} - \mathbf{G}_* \tag{7c}$$

For (7a) to hold, either $\mathbf{u_0} = \boldsymbol{\Gamma}$ or the difference $\boldsymbol{\Gamma} - \boldsymbol{u_0}$ must lie in the null space of $\mathbf{A}$ (6x6). In either of these cases, by satisfying (7a) we can ensure that the controlled level-ground gait replicates the passive trajectory.

However, as with most legged robots, the passive biped is underactuated, with control only over the rotational DoF:

$$\mathbf{u_0} = [0, 0, u_{\theta 1f}, u_{\theta 1k}, u_{\theta 2f}, u_{\theta 2k}]^T \tag{8}$$

Since $\boldsymbol{\Gamma}$ is a 6×1 vector with nonzero elements (because $a_* \neq 0$), the trivial solution $\mathbf{u_0} = \boldsymbol{\Gamma}$ is not admissible.

However, as shown in [19], the matrix $\mathbf{A}$ has $\mathrm{rk}(\mathbf{A}) = (6 - j)$ and therefore an j-dimensional null space. For the passive trajectory of interest (without DSP due to leg stiffness), $j = 2$, hence $\mathrm{rk}(\mathbf{A}) = 4$, and therefore $\mathbf{A}$ has a null space of dimension 2. Let $\mathbf{x_1}$ and $\mathbf{x_2}$ span the null space of $\mathbf{A}$; then we find that $\mathbf{u_0}$ satisfies (7a) when:

$$\mathbf{\Gamma} - \mathbf{u_0} = k_1\mathbf{x_1} + k_2\mathbf{x_2} \tag{9}$$

with arbitrary scalars k_1 and k_2. This results in a system of 6 equations in 6 unknowns (the 4 elements of $\mathbf{u_0}$ plus the two scalars k_1, k_2), which has a unique solution when $\mathbf{u_0}$ includes four independent components. Hence, a gravity-compensating control law is only feasible if four independent actuators are available.

C. Active biped

The passive biped is capable of stable walking on slopes in the range $a_* \in [-0.95°, -0.45°]$ [20]; here, an intermediate value $a_* = -0.6°$ is chosen for demonstration. The UVG torques $\mathbf{u_0}$ required for level-ground walking are computed by solving (9) at each timestep. Fig. 2a shows the femoral components $u_{\theta 1f}$, $u_{\theta 2f}$ of $\mathbf{u_0}$ during level-ground walking.

A common actuation strategy is to use a single actuator between the two femoral links [23] which only requires three motors. However, as Fig. 2a shows, here the required femoral torques differ in magnitude, necessitating four independent actuators. Notably, the negative sum of the femoral torques,

$$u_c = -(u_{\theta 1f} + u_{\theta 2f}) \tag{10}$$

remains nearly constant over the gait cycle (Fig. 2b). This observation motivates an active biped design that includes a torso link at the hip (Fig. 1d) to host the independent actuators. The torso, modeled as a link of length l_c, with a point mass m_c at a distance r_c from the hip and at an angle θ_c from the horizontal, experiences a gravitational torque:

$$w_c = m_c g l_c \cos(\theta_c) \tag{11}$$

Neglecting coupling terms (i.e., $f_c \approx 0$), its dynamics are approximated by:

$$(I_c + m_c l_c^2)\ddot{\theta}_c + \overset{0}{\cancel{f_c}} = u_c - w_c \tag{12}$$

By adopting a torso design that satisfies $m_c g l_c > u_c$, for some torso angle θ_{c_*} it will hold that $w_c \approx u_c$: this is true around two positions θ_{c_*}, one positive and one negative, see Fig. 3a. Although fluctuations in w_c and u_c mean that this balance is only approximate, the torso can be designed to ensure stable dynamics. For example, by positioning the torso in the 4^{th} quadrant (Fig. 3b), a self-correcting mechanism is created, as demonstrated in Fig. 3a. When $u_c > w_c$, based on (12), the angle θ_c is accelerated and tends to increase, see the mauve arrows in Fig. 3a. On the other hand, $u_c < w_c$ leads to a deceleration of θ_c, which will eventually decrease; see the blue arrows in Fig. 3a. These arrows demonstrate that the equilibrium around $\theta_{c_*} < 0$ is inherently stable, but unstable for $\theta_{c_*} > 0$, see Fig. 3c.

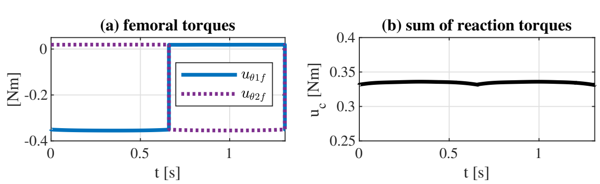

Figure 2. (a) The femoral torques $u_{\theta 1f}$, $u_{\theta 2f}$ required for level-ground walking with are not equal to each other. (b) The sum of reaction torques u_c is almost constant throughout the gait. Diagrams correspond to $a_* = -0.6°$ in the UVG, which leads to a horizontal walking velocity $v = 0.3$ m/s.

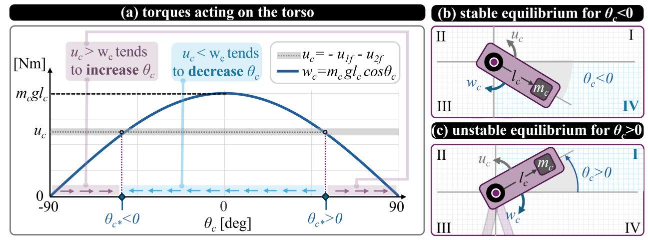

Figure 3. CW design: (a) Relationship between motor and gravitational torque u_c and w_c that act on the biped's torso and indication of stable and unstable equilibria. (b) Stable equilibrium in the 4^{th} quadrant, (c) unstable equilibrium in the 1^{st} quadrant.

A stable equilibrium around $\theta_{c_*} < 0$ will ensure that $w_c \approx u_c$ and therefore from (9) $\ddot{\theta}_c \approx 0$, which will in turn justify the simplification made in (12), as the coupling terms f_c only become significant with large velocities and accelerations.

The introduction of a torso link in Fig. 1d adds a fifth body, thereby enabling the incorporation of four independent actuators to control the original design's four rotational DoF according to the virtual gravity framework. The additional torso is designed to inherently maintain stability by balancing the femoral motors reaction torque, u_c, with the gravitational torque, w_c, acting on it.

Using the UVG, the new system replicates the dynamic behavior of the original passive biped. The control input is:

$$\mathbf{u} = [0, 0, u_{\theta 1f}, u_{\theta 1k}, u_{\theta 2f}, u_{\theta 2k}, -(u_{\theta 1f} + u_{\theta 2f})]^T \tag{13}$$

where the last element represents the torso actuation, constituting the reaction of the two femoral torques. The UVG controller, $\mathbf{u}$, is a *model-based* controller, computed analytically. It requires only an estimate of the biped's parameters and real-time feedback of the generalized coordinates $\mathbf{q}$.

Fig. 4 illustrates the evolution of the biped's knee and femoral states, sampled at the onset of each step under UVG control of the active biped on level ground. The plots demonstrate stable convergence of the states towards their respective limit cycles, showcasing the effectiveness of the UVG in harnessing the nonlinear passive gait dynamics. More details on the UVG's robustness, validation, and its efficacy in replicating passive gait can be found in [19].

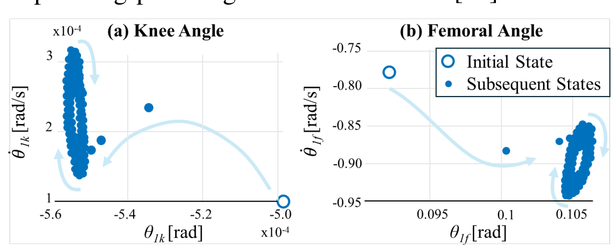

Figure 4. Inherent stability of the UVG. Convergence of the (a) knee and (b) femoral states at the beginning of each step, towards stable limit cycles, when starting from initial conditions that lie outside the limit cycle.

III. Optimal Control for Benchmarking the UVG

Here we present an optimal control strategy, to assess the efficiency and performance of the UVG via comparisons with numerically optimal controllers. The method numerically identifies an optimal open-loop trajectory using Trajectory Optimization (TOPT for planning), and tracks it using Nonlinear Model Predictive Control (NMPC for tracking).

A. TOPT for trajectory planning

The robot's numerically optimal walking trajectory is first planned via trajectory optimization. The trajectory optimization library OptimTraj [24] is employed to determine an open-loop trajectory that minimizes energy expenditure J, subject to the robot's dynamics and other desired gait attributes that are defined as optimization constraints.

To utilize the OptimTraj library, the robot's dynamics are expressed in explicit form, by using (3) to replace λ_0 in (5), which is then solved for $\ddot{\mathbf{q}}$. For the state $\mathbf{x} = [\mathbf{q}^\mathbf{T}, \dot{\mathbf{q}}^\mathbf{T}]^\mathbf{T}$:

$$\dot{\mathbf{x}} = \begin{bmatrix} \dot{\mathbf{q}} \\ \ddot{\mathbf{q}} \triangleq \boldsymbol{f}(\mathbf{x}, \mathbf{u}) \end{bmatrix} \tag{14}$$

where:

$$\boldsymbol{f}(\mathbf{x}, \mathbf{u}) = \mathbf{M}^{-1}\big((\mathbf{I} - \mathbf{J}\boldsymbol{\Delta}\mathbf{J}^\mathbf{T}\mathbf{M}^{-1})(\mathbf{u} - \mathbf{C} - \mathbf{G_0}) - \mathbf{J}\boldsymbol{\Delta}\dot{\mathbf{J}}^\mathbf{T}\dot{\mathbf{q}}\big) \tag{15}$$

The optimization problem is defined as:

$$\begin{aligned} \min_{\mathbf{u}(t), \mathbf{x}(t), T} \quad & J = \int_0^T \mathbf{u}^2(\tau)\, d\tau \\ \text{s.t.} \quad & \dot{\mathbf{x}}(t) = \boldsymbol{f}(\mathbf{x}(t), \mathbf{u}(t)) \\ & \mathbf{s}(\mathbf{x}) = 0, \qquad \mathbf{g}(\mathbf{x}(0), \mathbf{x}(T)) = 0 \\ & \mathbf{h}(\mathbf{x}(t), \mathbf{u}(t)) > 0, \quad \mathbf{c}(\mathbf{x}(t), \mathbf{u}(t), T) < 0 \end{aligned} \tag{16}$$

The trajectories must satisfy the system dynamics $\boldsymbol{f}$ in (14), which are introduced in the optimization as constraints linking $\mathbf{x}(t)$ and $\mathbf{u}(t)$. The stance foot constraints $\mathbf{s}$ are obtained from (2b) and their analytical derivation can be found in [21]. Furthermore, three types of optimization constraints are introduced: boundary equality constraints $\mathbf{g}$, path inequality constraints $\mathbf{h}$ and decision variable bound constraints $\mathbf{c}$. These are detailed in the following.

First, a requirement for gait repetitiveness g_1 is imposed by equating each step's initial and final states:

$$g_1 = \mathbf{x}(0) - \mathbf{W}\mathbf{x}(T)^+ = 0 \tag{17}$$

where $\mathbf{x}(T)^+$ is the state after the heelstrike impact and $\mathbf{W}$ performs the switch between the left and right legs. The impact is modeled as an inelastic collision [25]:

$$\begin{bmatrix} \dot{\mathbf{q}}(T)^+ \\ \int_{T^-}^{T^+} \lambda(t)\, dt \end{bmatrix} = \begin{bmatrix} \mathbf{M} & -\mathbf{J} \\ \mathbf{J^T} & \mathbf{0} \end{bmatrix}^{-1} \begin{bmatrix} \mathbf{M}\dot{\mathbf{q}}(T)^- \\ \mathbf{0} \end{bmatrix} \tag{18}$$

with post-impact velocities $\dot{\mathbf{q}}(T)^+$ calculated by applying the conservation of angular momentum [26]. The matrix inversion in (18) is always possible as $\mathbf{M}$ is positive definite and $\mathbf{J}$ is full column rank [25]. Positions are continuous before and after the instantaneous impact, $\mathbf{q}(T)^+ = \mathbf{q}(T)$, and finally:

$$\mathbf{x}(T)^+ = [\mathbf{q}(T)^T, \dot{\mathbf{q}}(T)^+]^T \tag{19}$$

The performance of repetitive steps as imposed by g_1 ensures a sustainable cyclic gait.

Next, a desired walking velocity is set by g_2 constraining the ratio of the total horizontal hip displacement x_h over the step's temporal duration T to be equal to a desired v:

$$g_2 = \frac{x_h(T) - x_h(0)}{T} - v = 0 \tag{20}$$

The walking velocity constraint ensures that similar gaits are compared across the two methods.

A swing foot inequality constraint h_1 ensures that the swing foot does not scuff the ground:

$$h_1 = y_c(t) > 0 \text{ , for t} \in \text{(0,T)} \tag{21}$$

where y_c is the swing foot's distance from the ground, with [21] presenting the details of its calculation for any convex foot shape. Knee cap inequality constraints h_2, h_3 are imposed to avoid knee hyperextension:

$$h_2 = \theta_{1k}(t) \geq 0 \tag{22}$$

$$h_3 = \theta_{2k}(t) \geq 0 \tag{23}$$

Finally, $\mathbf{c}$ imposes upper and lower bounds for the elements of $\mathbf{x}$, $\mathbf{u}$ as well as for the step duration T.

The library uses direct collocation with N points to numerically calculate an open-loop trajectory that minimizes J. The N collocation points are equally spaced in time, spanning the range $[0, T]$. In this work, the continuous integral J as well as the state derivatives $\dot{\mathbf{x}}_k$ are approximated via trapezoidal quadrature for all collocation points $k \in [0, N]$. Increasing N improves the feasibility of the trajectories by ensuring that the system dynamics and constraints are satisfied in more instances across the trajectory. However, this leads to an increase in computational cost and longer convergence times. Here, two consecutive passes are performed: first, a coarse pass with $N = 15$ is used to quickly converge towards the optimal trajectory, followed by a detailed pass that uses $N = 40$ collocation points for each step.

The trajectory obtained from the optimization process is an open-loop trajectory that provides time series for the control inputs $\mathbf{u}$ and the state variables $\mathbf{x}$. This trajectory is computed offline to locally satisfy the system dynamics and the imposed constraints at the collocation points. However, because it is generated in an open-loop manner, any perturbations or modeling inaccuracies can lead to deviations from the desired behavior. To robustly track such trajectories in practice, real-time feedback controllers are essential to stabilize the system and compensate for disturbances.

B. NMPC for trajectory tracking

Subsequently, the TOPT-computed open-loop trajectory is tracked using NMPC. The employed NMPC continuously refines control actions by solving an online optimization problem of a nonlinear system that accounts for nonlinear constraints, thus ensuring that the robot follows the optimized trajectory as closely as possible.

For the current step k, the NMPC calculates an optimal control input sequence $\mathbf{u}_{k:k+m}$, with a control horizon $m = 2$ for a prediction horizon $p = 3$, with a sampling time $T_s = 0.025s$, solving a temporally local version of the optimization problem defined in (16), as presented in (24):

$$\begin{aligned} \min_{\mathbf{u}_{k:k+m}} \quad & \sum_{i=k}^{k+p-1} (\mathbf{e}_i^T \mathbf{Q}_i \mathbf{e}_i + \mathbf{u}_i^T \mathbf{R}_i \mathbf{u}_i) \\ \text{s.t.} \quad & \mathbf{x}_{i+1} = f_d(\mathbf{x}_i, \mathbf{u}_i), \quad \mathbf{s}(\mathbf{x}_i) = 0 \\ & \mathbf{h}(\mathbf{x}_i, \mathbf{u}_i) > 0, \quad \mathbf{c}(\mathbf{x}_i, \mathbf{u}_i) < 0 \end{aligned} \tag{24}$$

where $\mathbf{e}_i$ is the error between the reference trajectory and the predicted system response, for i spanning the prediction horizon. $\mathbf{Q}_i$ and $\mathbf{R}_i$ are positive-definite weight matrices, different for each prediction step, allowing the variation of optimization weights across the trajectory.

Compared to the non-linear program (16) used in trajectory optimization, the MPC problem is discretized, with a discrete formulation of the system dynamics f_d. Also, it includes the path inequality constraints $\mathbf{h}$ and decision variable bounds $\mathbf{c}$, without considering the boundary equality constraints $\mathbf{g}$, as the overall step trajectories are already planned in the trajectory optimization phase.

The success of the NMPC controller in tracking the TOPT trajectory is demonstrated in Fig. 5, which shows the joint angles (a-e), angular velocities (f-j) and joint torques (k-n) during one step of the biped. The plot compares the open-loop TOPT trajectory, captured at $N = 40$ collocation points, with the actual trajectory that is performed when the NMPC is used to stabilize the TOPT output. The plots demonstrate that the biped successfully follows the TOPT state trajectories, with the torques presenting brief corrective deviations from the TOPT open-loop values, that minimize errors and stabilize the trajectory. Notably, the 4-input NMPC controller stabilizes the TOPT trajectory in all the 10 states.

C. Comparison Methodology

The benchmarking of the developed UVG controller is based on systematic comparisons with the TOPT + NMPC scheme detailed above, as described in Algorithm 1.

The comparative approach provides insights into the advantages and limitations of the UVG controller relative to TOPT+NMPC, highlighting aspects such as energy efficiency and computational complexity.

IV. Results

The benchmarking methodology described in Algorithm 1 is applied to the biped robot across a range of walking velocities from $v = 0.1$ m/s to $v = 0.5$ m/s. In this section, we first present a detailed analysis of the gaits achieved comparing the methods at a representative walking velocity $v = 0.3$ m/s. Subsequently, we provide a comprehensive comparison of the two methods across the full range of walking velocities, covering a variety of gait patterns where the methods may exhibit varying behaviors.

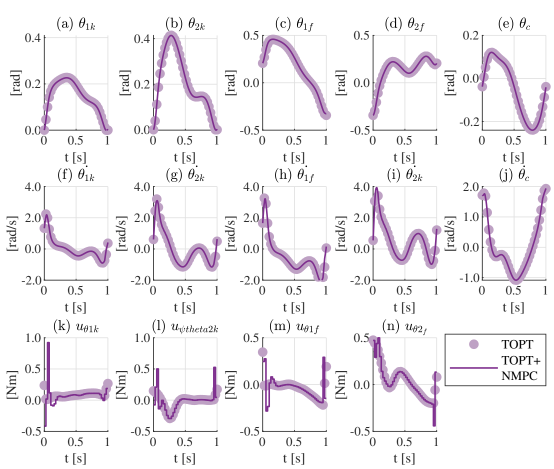

Figure 5. NMPC controller successfully tracks TOPT generated trajectory for forward walking velocity $v = 0.3m/s$, as illustrated by the joint angles (a-e), angular velocities (f-j) and joint torques (k-n) of the biped.

A. Detailed Comparison at a Constant Walking Speed

For a set walking velocity $v = 0.3$ m/s the TOPT+NMPC method described above is used to provide an energetically efficient walking trajectory and stabilize it. The temporal progression of TOPT and NMPC trajectories have been presented in Fig. 5 which showcased successful tracking achieved by the NMPC controller. The repeatability of the achieved gait is demonstrated in Fig. 6, which plots the phase plane of the femoral, knee and torso angles across the TOPT+NMPC trajectory with a purple dashed line.

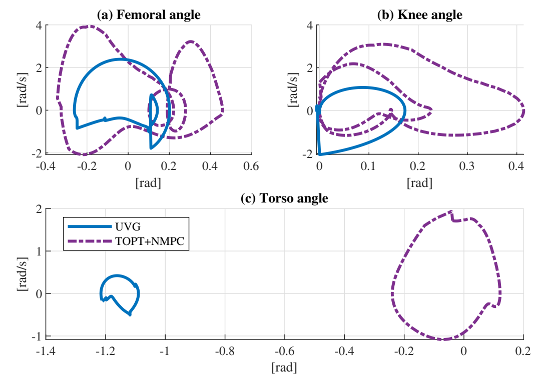

Figure 6. Phase plane comparisons for (a) the femoral (θ_f), (b) knee (θ_k) and (c) torso (θ_c) angles of the biped under UVG and TOPT+NMPC implementations. Horizontal walking velocity $v = 0.3m/s$.

The TOPT+NMPC trajectory is compared with the trajectory that results from the use of the UVG controller for the same walking velocity. The UVG trajectory is plotted in Fig. 6 with a continuous blue line.

Both trajectories are cyclic, constituting repetitive gait cycles for level-ground walking at the same speed. The major difference between the two trajectories is observed in the torso angle, where TOPT has converged to an almost-zero torso angle as the optimal trajectory, while UVG requires that the torso lies in the 4^{th} quadrant for inherent stability.

Another important difference between the two methods lies

Algorithm 1 UVG Benchmarking Procedure

---

for a_* in $\mathbb{A}^*$ **do**
  Perform walking using UVG control (9) and (13).
  Store the UVG trajectory, $\mathcal{T}_{UVG}$.
  Measure UVG horizontal walking velocity, v_{UVG}.
  Compute evaluation metrics.
end for
Let $\mathbb{V}^*$ be the set of achieved v_{UVG}.
for v_{des} in range $[min(\mathbb{V}^*)/1.20, max(\mathbb{V}^*) \times 1.20]$ **do**
  if UVG walking exists with $v_{UVG} \approx v_{des}$ **then**
    Use $\mathcal{T}_{UVG}$ as the initial guess in (16).
  else
    Use the previously computed $\mathcal{T}_{TOPT}$.
  end if
  Solve the TOPT problem (16).
  Store the optimized trajectory, $\mathcal{T}_{TOPT}$.
  Track $\mathcal{T}_{TOPT}$ in real time using NMPC (24).
  Store the performed trajectory, $\mathcal{T}_{NMPC}$.
  Compute evaluation metrics.
end for
Compare UVG and TOPT+NMPC implementations of level-ground walking across different velocities.

---

in the range of joint angles and their velocities, where the TOPT+NMPC approach demonstrates a larger variation of these measures for the same walking velocity, as indicated by the areas that are occupied by the corresponding plots.

Next, the mechanical power consumed by the two controllers is calculated and plotted in Fig. 7a-d for the 4 motors of the biped. In the knee joints (a and b) the UVG controller barely draws any power, in contrast with the TOPT+NMPC implementation which leads to significant power peaks. The femoral motors are more energy consuming in both controllers; however the overall mechanical power levels are smaller with the UVG compared to the TOPT+NMPC. The surfaces below the power curve are highlighted in the plots, as they are directly linked to the energetic consumption. Visual inspection of Fig. 7 implies that the purple areas are greater than the blue ones, hinting at an increased energetic consumption of TOPT+NMPC.

This observation can be quantified by calculating the Cost of Transport (COT). For a walking motion starting at t_0 and ending at t_f, where the total energy spent in the 4 motors is divided by the theoretical work of this forward progression:

$$\mathrm{COT} = \frac{\sum_{i=1}^{4} \int_{t_0}^{t_f} |u_i(t) * \omega_i(t)| dt}{Mg(x_h(t_f) - x_h(t_0))} \tag{25}$$

where u_i is the input torque of the the i^{th} motor and ω_i is the relative angular velocity of the joint around which this torque is applied. Evaluating the COT for 10 steps of each of these gaits provides the following results:

$$\begin{aligned} \mathrm{COT}_{\mathrm{UVG}} &= 0.017 \\ \mathrm{COT}_{\mathrm{TOPT+NMPC}} &= 0.025 \end{aligned} \tag{26}$$

Both of these COT values correspond to the same biped walking with a horizontal walking velocity $v = 0.3$ m/s. The findings indicate that UVG control is 32% more efficient than the TOPT+NMPC control for this walking velocity. This is consistent with the initial observations of relatively contained joint motions and smaller joint velocities of the UVG in comparison with the TOPT+NMPC in Fig. 6, and with the reduced mechanical power consumption evident in Fig. 7.

The reason for this improvement lies in the inherent exploitation of the passive walking dynamics by the UVG controller: since the biped can passively walk down small slopes with no motor input, the input required to compensate

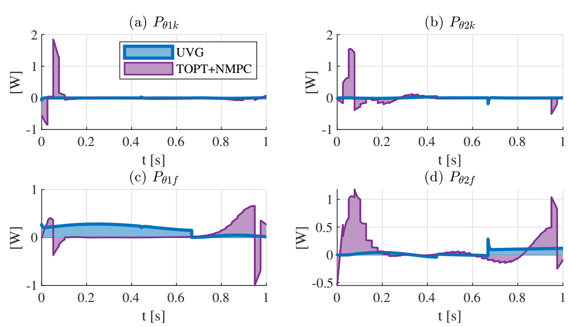

Figure 7. Comparison of mechanical power consumption across one step of the TOPT+NMPC biped, with a duration $\Delta t = 1s$. UVG power consumption demonstrated across 1.5 steps of the biped (UVG step duration $\Delta t = 0.67s$). Both gaits have a common walking velocity $v = 0.3m/s$.

for the level ground is very small and linked to the shift in gravity's direction [22]. This implies that the limitations of passive walking, mainly the limited range of velocities due to the slope angles where passive walking is possible, will extend to the UVG. This is explored in the next section where the comparison is extended to a range of walking velocities.

B. Comparison of range metrics

To perform the comparisons across a wide range of walking velocities, we follow Algorithm 1, investigating the performance of the UVG controller for various $a_* \in \mathbb{A}^*$ as the slope parameter for the UVG control scheme. The set of walking velocities, v_{UVG}, achieved constitutes $\mathbb{V}^*$. Next, we apply the TOPT+NMPC scheme for a range of walking velocities that is $\pm 20\%$ of the range of velocities in $\mathbb{V}^*$. The resulting sets of gaits are then compared to each other.

Fig. 8 presents the mean value of the torso angle, θ_c, during walking, along with its minimum and maximum values recorded, for various walking velocities. The figure displays the variations of θ_c for the UVG and TOPT+NMPC implementations of level-ground walking. Fig. 6c constitutes a cross-section of the plot in Fig. 8 for $v = 0.3$ m/s.

A first look at the figure indicates that the UVG control scheme is able to perform level-ground walking with velocities ranging from $v = 0.23$ m/s to $v = 0.42$ m/s, while the TOPT+NMPC scheme finds solutions for the entire range of the velocities considered.

The set of velocities where both controllers provide repetitive gaits can be divided in two: for $v < 0.27$ m/s the torso angle θ_c exhibits smaller variations under the TOPT+NMPC control compared to the UVG control. For higher velocities, the range of θ_c using UVG becomes significantly smaller than the one with TOPT+NMPC, indicating increased torso stabilization. This effect is more pronounced for $v = 0.32$ m/s where the torso presents a minimal motion $\pm 5°$ for the UVG, while for the TOPT+NMPC this range is $\pm 10°$.

Next we compare the joint torques between the two schemes. Fig. 9 presents the mean value and range of joint torques for the UVG and the TOPT+NMPC implementation, for various walking velocities.

As observed in Fig. 9 the UVG control requires joint torques that are almost constant around a central value, which has been demonstrated already in Fig. 2a for $v = 0.3$ m/s. In contrast, the torques in the TOPT+NMPC implementation present large fluctuations while preserving the mean torque value close to zero. This is also evident in Fig. 5k-n for

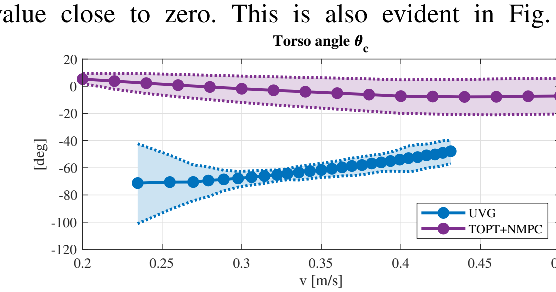

Figure 8. Torso angle: mean value and range for stable gaits across a range of walking velocities. Comparison for the two control schemes.

$v = 0.3$ m/s. This observation holds across the common range of walking velocities of the two implementations, but becomes more pronounced for increased velocities.

The large angular displacements and increased joint torques of the TOPT+NMPC implementation hint at an increased energetic consumption when compared to the UVG control. To validate this, the COT for 10 consecutive steps is calculated for both implementations, using (25), with results in Fig. 10.

In addition to the UVG and TOPT+NMPC implementations, the figure also demonstrates the theoretical estimation of the UVG COT, which is equal to $sin(|a_*|)$[22], along with the COT estimation for the TOPT-generated trajectory prior to its stabilization with the NMPC.

Comparing the UVG COT to its theoretical value, it is observed that for most of the velocities in $\mathbb{V}^*$, the two are almost coincident. Small variations are due to the fact that the absolute value of motor power is used in the calculation of COT in (25), while in passive walking the torques are generated by gravitational forces, which are conservative meaning that their net work in a closed loop is zero. A large deviation is observed for small walking velocities, where the UVG scheme is somehow underperforming, as observed by the large angular motions observed in Fig. 8. Due to the low performace of the UVG in low velocities, the UVG curve presents a COT minimum at $v = 0.28$ m/s.

Additionally, it is observed that while NMPC succeeds in stabilizing the TOPT open-loop trajectory, this leads to an increasingly higher COT compared to the TOPT predictions.

Most importantly, Fig. 10 shows that apart from the low-performing velocities $v < 0.25$ m/s, the UVG control outperforms both the TOPT open-loop trajectory and the TOPT+NMPC stabilized implementation, providing an efficient option for level-ground walking.

V. Discussion

Comparisons between the proposed UVG control and the alternative TOPT+NMPC were conducted both at a specific walking velocity and across a range of walking speeds.

The results demonstrate that the UVG method yields simpler and more contained joint motions, characterized by minimal movement in the biped's active DoF and reduced peak torques

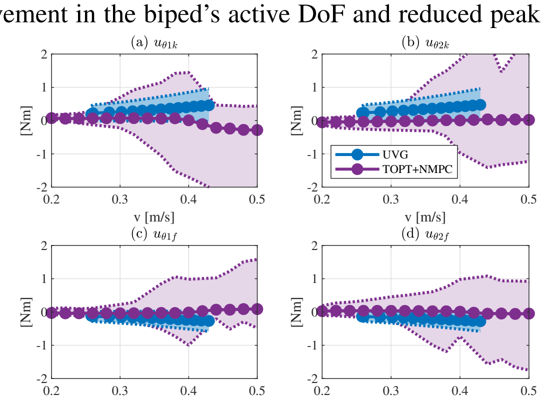

Figure 9. Joint torques comparison for the UVG and TOPT+NMPC control schemes for various walking velocities.

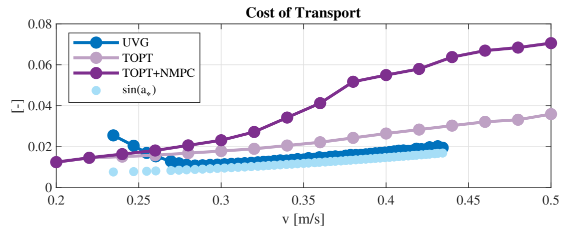

Figure 10. COT achieved in level-ground walking across various walking velocities. UVG and TOPT+NMPC implementations are compared to their theoretical values and to each other, where the UVG controller outperforms TOPT+NMPC for a special range of velocities.

compared to the TOPT+NMPC implementation. This reduction in state variation, as illustrated in Fig. 6 and Fig. 8, hints at a lower COT and suggests a broader applicability of the UVG scheme, particularly for robots with mechanical constraints in their DoF. While TOPT can be configured to enforce limits on state variables, this constraint would exclude the identified optimal solutions presented in this study, resulting in increased energy consumption.

The UVG's reduced peak torques, shown in Fig. 2, Fig. 5, and Fig. 9, enable the potential use of lighter-weight actuators, which can enhance robot efficiency and simplify mechanical design. The UVG's lower power consumption, evident in Fig. 7 for $v = 0.3$ m/s, further supports the feasibility of employing less powerful actuators, contributing to improved energy efficiency.

Notably, the UVG demonstrated superior energetic efficiency within a specific range of walking velocities. As shown in Fig. 10, the corresponding COT is smaller for $u \in [0.27, 0.42]$ m/s, confirming the energetic advantage of the UVG over the TOPT+NMPC in this region.

The results highlight the UVG's effectiveness in achieving stable and efficient level-ground walking. In addition, its effectiveness is enhanced by the fact that it constitutes a closed-form solution, offering a computational advantage over numerical methods such as the TOPT+NMPC: indeed, the UVG only requires calculation of the algebraic feedback law once at each time step and is therefore $\mathcal{O}(n)$; while for the same time step the TOPT/NMPC approach requires calculations of $\mathcal{O}(n^3)$ for forward dynamics and their derivatives [8], over the horizon p, *iteratively* i times until numerical convergence, leading to $\mathcal{O}(ipn^3)$.

The benchmarking of the UVG was carried out through comparisons with methods that explicitly target optimality, such as the TOPT+NMPC. The superior efficiency of the UVG demonstrated in this paper, suggests that the *numerical* search for optimality does not necessarily indicate the optimal approach. This is largely due to the nonlinear nature of the dynamics and the fact that they are only evaluated at discrete collocation points, while passive dynamics can only be simulated through dense temporal sampling. The UVG highlights that dynamics-based and design-aware approaches can uncover valuable alternatives in the pursuit of optimality.

Note that the UVG's applicability is restricted to a specific range of walking velocities. This limitation aligns with established findings in passive walking studies, which indicate that the achievable horizontal velocity in passive walking is inherently limited by the robot's design characteristics [27]. As the UVG relies on the robot's capacity to perform passive gaits, this limitation naturally carries over. Conversely, the TOPT+NMPC approach can accommodate a wider range of gait velocities, at the cost of increased power expenditure.

Despite this constraint, the UVG, along with similar methods that exploit a robot's natural dynamic tendencies, presents a powerful control framework. By embracing passivity, robots may achieve enhanced power autonomy and improved energy efficiency in their primary tasks. Meanwhile, universally applicable approaches such as TOPT+NMPC can extend the robot's operational range, offering a complementary solution for conditions where passive dynamics alone may fall short. Together, these strategies highlight the exciting potential for robots that skillfully balance natural dynamics and advanced control methodologies, paving the way for more adaptable, capable, and efficient robotic systems.

It is important to note that the UVG is a controller for the steady-state walking of biped robots. An immediate next step of this work is the investigation of starting and stopping trajectories for the robot to transition between rest and this steady-state. Following this, we plan to validate the performance of real-world experiments to validate the efficiency of the UVG controller and the results of the comparative approach.

VI. Conclusion

This work explored and benchmarked the UVG control scheme, highlighting its ability to harness passive dynamics for energy-efficient bipedal walking. By promoting natural motion patterns, reducing actuator effort, and achieving superior energy performance, the UVG presents a powerful solution for efficient locomotion. Its effectiveness within a specific velocity range demonstrates that robotic systems can be purposefully designed to resonate with passive dynamic behaviors, enhancing inherent stability and minimizing energy use. By embracing passive dynamics as a core design principle, and complementing passivity-based controllers with versatile approaches such as TOPT+NMPC, future robotic systems may achieve unprecedented efficiency, robustness, and adaptability, unlocking new potential in real-world environments.

References

[1] K. Erbatur and O. Kurt, "Natural ZMP Trajectories for Biped Robot Reference Generation," *IEEE Transactions on Industrial Electronics*, 2009, vol. 56, no. 3, pp. 835-845.

[2] T. Sugihara et al., "Real-time humanoid motion generation through ZMP manipulation based on inverted pendulum control," *IEEE Int. Conf. on Rob. and Autom.*, Washington, DC, USA, 2002, vol.2, pp. 1404-1409.

[3] A. Meduri et al., "BiConMP: A Nonlinear Model Predictive Control Framework for Whole Body Motion Planning," *IEEE Transactions on Robotics*, 2023, vol. 39, no. 2, pp. 905-922.

[4] E. Daneshmand et al., "Variable Horizon MPC With Swing Foot Dynamics for Bipedal Walking Control," *IEEE Robotics and Automation Letters*, 2021, vol. 6, no. 2, pp. 2349-2356.

[5] E. R. Westervelt, J. W. Grizzle and D. E. Koditschek, "Hybrid zero dynamics of planar biped walkers," *IEEE Trans. on Automatic Control*, 2003, vol. 48, no. 1, pp. 42-56.

[6] J. W. Grizzle, C. Chevallereau and Ching-Long Shih, "HZD-based control of a five-link underactuated 3D bipedal robot," *IEEE Conference on Decision and Control*, Cancun, Mexico, 2008, pp. 5206-5213.

[7] A. Hereid, *et al*, "3D dynamic walking with underactuated humanoid robots: A direct collocation framework for optimizing hybrid zero dynamics," *IEEE Int. Conf. on Robotics and Automation*, Stockholm, Sweden, 2016, pp. 1447-1454.

[8] J. N. Nganga and P. M. Wensing, "Accelerating Second-Order Differential Dynamic Programming for Rigid-Body Systems," *IEEE Rob. and Autom. Letters*, vol. 6, no. 4, pp. 7659-7666, Oct. 2021.

[9] H. Duan, J. Dao, K. Green, T. Apgar, A. Fern and J. Hurst, "Learning Task Space Actions for Bipedal Locomotion," *IEEE Int. Conference on Robotics and Automation*, Xi'an, China, 2021, pp. 1276-1282.

[10] X. Da, R. Hartley and J. W. Grizzle, "Supervised learning for stabilizing underactuated bipedal robot locomotion, with outdoor experiments on the wave field," *IEEE International Conference on Robotics and Automation*, Singapore, 2017, pp. 3476-3483.

[11] A. Goswami, B. Espiau and A. Keramane, "Limit Cycles in a Passive Compass Gait Biped and Passivity Mimicking Control Laws," *Autonomous Robots*, 1997, vol. 4,no. 3, pp. 273-286.

[12] M. W. Spong, J.K. Holm, D. Lee, "Dynamics of Bipedal Locomotion Passivity-Based Control of Bipedal Locomotion Regulating Walking by Exploiting Passive Gaits in 2-D and 3-D Bipeds," *IEEE Robotics and Automation Mag.*, 2007, vol. 14, no. 2, pp. 30-40.

[13] H. Sasaki and M. Yamakita, "Efficient Walking Control of Robot with Torso Based on Passive Dynamic Walking," *IEEE Int. Conf. on Mechatronics*, 2009, pp. 113-120.

[14] Y. Hu, G. Yan, Z. Lin and M. Liu, "Time-scaling control and passive walking of bipeds with underactuation degree one," *IEEE Conference on Decision and Control*, Atlanta, GA, USA, 2010, pp. 1116-1121.

[15] C. Chevallereau, "Time scaling control for an underactuated biped robot", *IEEE Transactions on Robotics and Automation*, 2003, vol. 19, no. 2, pp. 362-368.

[16] J. Pratt and G. Pratt, "Intuitive control of a planar bipedal walking robot," *IEEE International Conference on Robotics and Automation*, Leuven, Belgium, 1998, pp. 2014-2021.

[17] Steve Collins et al., "Efficient Bipedal Robots Based on Passive-Dynamic Walkers", *Science*, 2005, 307, pp. 1082-1085.

[18] Bhounsule PA, Cortell J, Grewal A, et al. Low-bandwidth reflex-based control for lower power walking: 65 km on a single battery charge. *The International Journal of Robotics Research*, 2014, 33(10).

[19] D. Maligianni, F. Valouxis, A. Kantounias, A. Smyrli, and E. Papadopoulos, "A Virtual Gravity Controller for Efficient Underactuated Biped Robots," *IEEE International Conference on Robotics and Automation*, Atlanta, GA, USA, 2025, pp. 7668-7674.

[20] A. Smyrli and E. Papadopoulos, "Improved biped walking performance around the kinematic singularities of biomimetic four-bar knees," *IEEE/RSJ Int. Conf. on Intelligent Robots and Systems*, Kyoto, Japan, 2022, pp. 6774-6779.

[21] A. Smyrli and E. Papadopoulos, "A methodology for the incorporation of arbitrarily-shaped feet in passive bipedal walking dynamics," *IEEE Int. Conf. on Robotics and Autom.*, Paris, France, 2020, pp. 8719-8725.

[22] A. Smyrli, M. Ghiassi, A. Kecskeméthy and E. Papadopoulos, "On the effect of semielliptical foot shape on the energetic efficiency of passive bipedal gait," *IEEE/RSJ Int. Conf. on Intelligent Robots and Systems,* Macau, China, 2019, pp. 6302-6307.

[23] X. Xiao, O. Ma and F. Asano, "Control walking speed by approximate-kinetic-model-based self-adaptive control on underactuated compass-like bipedal walker," *IEEE Int. Conf. on Robotics and Automation*, 2017, Singapore, pp. 4729-4734.

[24] M. Kelly, "An introduction to trajectory optimization: How to do your own direct collocation," *SIAM review*, 2017, vol.59, no.4, pp.849-904.

[25] J. W. Grizzle, G. Abba and F. Plestan, "Asymptotically stable walking for biped robots: analysis via systems with impulse effects," *IEEE Transactions on Automatic Control*, 2001, vol. 46, no. 1, pp. 51-64.

[26] Y. Hurmuzlu, and D.B. Marghitu, "Rigid body collisions of planar kinematic chains with multiple contact points". *The International Journal of Robotics Research*, 1994, vol.13, no.1 , pp. 82-92.

[27] A. Smyrli, G. Bertos and E. Papadopoulos, "A generalized model for compliant passive bipedal walking: sensitivity analysis and implications on bionic leg design," *ASME Journal of Biomechanical Engineering*, 2021, vol. 143, no. 10.

Acknowledgment

This work is funded by the European Union under Horizon Europe (grant No. 101136568 - HERON).

Funded by the European Union